J Nanostruct 16(3): 3053-3068, Summer 2026

RESEARCH PAPER

Synthesis and Characterization of Xanthan Gum-g-poly (PVP-co-AA-AAm) Nanohydrogel for Efficient Removal of Brilliant Green Dye from Aqueous Solutions: Kinetics, Isotherms, and Thermodynamic Studie

Nagham H. Abood [1], Duaa Ayad Yass [2], Layth S. Jasim [3]*

[1] *Department of Applied Chemistry, College of Applied Sciences, University of Technology, Baghdad, Iraq*

[2] *Middle Technical University, Technical Institute-Baqubah, Diyala, Iraq*

[3] *Department of Chemistry, College of Education, University of Al-Qadisiyah, Diwaniyah, Iraq*

ARTICLE INFO

Article History:
Received 05 March 2026
Accepted 07 May 2026
Published 01 July 2026

Keywords:
Adsorption kinetics
Brilliant Green dye
Freundlich isotherm
Thermodynamics
Wastewater treatment
Xanthan gum nanohydrogel

ABSTRACT

Synthetic dyes are toxic, cancer-causing, and mutagenic, which makes water pollution a big environmental problem. This study synthesised a novel xanthan gum-grafted-poly(polyvinylpyrrolidone-co-acrylic acid-acrylamide) [XG-g-poly(PVP-co-AA-AAm)] nanohydrogel for the removal of Brilliant Green (BG) cationic dye using free radical graft copolymerisation. The XRD study showed an amorphous structure with semi-crystalline peaks at 19.18°, 20.68°, and 23.38°. These peaks were linked to xanthan gum, PVP, and polyacrylamide. FTIR confirmed that the grafting worked and found the functional groups (–OH, $–CONH_2$, $–COO^-$) that were responsible for binding the dye. The post-adsorption bands at 1514, 1712, and 1165 cm^{-1} show that BG was absorbed by electrostatic attraction and hydrogen bonding. Decomposition started at 234.3°C, and TGA/DTA was thermally stable at Tg = 79°C. FESEM indicated that the surfaces changed shape following adsorption, going from smooth (d = 75.4 nm) to spherical dye nanoparticle-covered surfaces (d=29.7–162.7 nm). The nanohydrogel could hold 37.33 mg/g and remove 93.34% of what it was supposed to in 90 minutes when the conditions were just right (C_0 = 200 mg/L, dose = 0.005 g, natural pH, T=30°C). The pseudo-second-order model (R^2=1.000) in kinetics proved that chemisorption was real. Weber-Morris forecasted the influence of boundary layer diffusion (C = 36.34 mg/g). The best fit equilibrium data using the Freundlich isotherm indicated heterogeneous multilayer adsorption. Thermodynamic studies showed that adsorption was spontaneous ($\Delta G° < 0$), endothermic ($\Delta H° > 0$), and unexpected ($\Delta S° > 0$). When we used NaCl, KCl, and $CaCO_3$ to test ionic strength, they all worked well even though there were other electrolytes. These studies indicate that nanohydrogel is an environmentally favourable adsorbent for cationic dye-contaminated wastewater.

How to cite this article
Abood N., Yass D., Jasim L. Synthesis and Characterization of Xanthan Gum-g-poly (PVP-co-AA-AAm) Nanohydrogel for Efficient Removal of Brilliant Green Dye from Aqueous Solutions: Kinetics, Isotherms, and Thermodynamic Studie. J Nanostruct, 2026; 16(3):3053-3068. DOI: 10.22052/JNS.2026.03.005

* *Corresponding Author Email: 100397@uotechnology.edu.iq*

INTRODUCTION

Globally, synthetic dyes from textile, paper, leather, and pharmaceutical sectors pollute water [1,2]. These dyes reduce light penetration, impede photosynthesis, and are harmful to aquatic creatures and humans even at low concentrations [3]. An estimated 10,000 dyes and pigments are used in industry, and 7×105 tonnes of synthetic dyes are generated annually, with a significant amount entering waterways through faulty effluent treatment [4]. Industrial discharges often contain Brilliant Green (BG), a cationic triphenylmethane dye used in silk and wool dyeing as a biological stain, antibacterial, and colourant [5]. BG can cause skin irritation, respiratory discomfort, and carcinogenicity with extended exposure [6]. The pressing need for effective and cost-effective BG removal from contaminated water bodies exists. Dye removal from wastewater has been studied using coagulation-flocculation, membrane filtering, electrochemical oxidation, photocatalytic degradation, and biological treatment [7,8]. These methods have drawbacks such high operational costs, secondary sludge, insufficient dye removal, and lack of scalability [9]. In contrast, adsorption has been popular as a versatile and cost-effective approach due to its simplicity, ease of operation, high efficiency, and adsorbent renewal [10,11]. Choosing the right adsorbent material is crucial to adsorption success. Researchers have developed low-cost, sustainable alternatives to activated carbon, which is effective but too expensive for large-scale use [12,13]. Due to its three-dimensional polymeric network, high water absorption capacity, variable functionality, and numerous surface-active sites, hydrogel-based adsorbents have garnered research attention [14,15]. Selecting monomers, crosslinkers, and natural polymer backbones can customise hydrogel adsorption [16]. We like natural polysaccharide-based hydrogels because they combine biodegradability and biocompatibility with synthetic polymer strength and swelling [17,18]. Anionic exopolysaccharide Xanthomonas campestris produces xanthan gum (XG) with a cellulose backbone and trisaccharide side chains with carboxylate and pyruvate groups [19]. Hydrogels benefit from its polyanionic nature, large molecular weight, and water solubility [20]. Grafting acrylic acid (AA), acrylamide (AAm), and polyvinylpyrrolidone (PVP) onto the XG backbone adds carboxyl, amide, and carbonyl moieties that increase hydrogel swelling and dye binding [21,22]. Past investigations have shown that polysaccharide-grafted hydrogels may remove heavy metals, anionic dyes, and cationic dyes [23–25]. Numerous research have examined dye adsorption using various adsorbents, but few have examined XG-based multicomponent hydrogels for Brilliant Green dye removal. To fill this gap, this study synthesises a new XG-g-poly(PVP-co-AA-AAm) nanohydrogel via free radical copolymerisation using potassium persulfate (KPS) as initiator and N,N'-methylenebisacrylamide (MBA) as crosslinker TGA/DTA, FESEM, XRD, and FTIR were used to characterise the nanohydrogel. Batch adsorption tests examined the effects of contact time, pH, adsorbent dosage, initial BG concentration, ionic strength, and temperature. To understand the adsorption mechanism and feasibility, pseudo-first-order [26] and pseudo-second-order [27] kinetic models, Langmuir [28], Freundlich [29], and Temkin [30] isotherm models, and thermodynamic parameters were used to analyse the experimental data.

MATERIALS AND METHODS

Materials

Xanthan gum (XG, molecular weight ~2 × 10^6 g/mol) was procured from Sigma-Aldrich. Polyvinylpyrrolidone (PVP, K-30 grade), acrylic acid (AA, 99%), acrylamide (AAm, ≥99%), potassium persulfate (KPS, ≥98%), N,N'-methylenebisacrylamide (MBA, 99%), and N,N,N',N'-tetramethylethylenediamine (TEMED) were obtained from Merck. Brilliant Green dye (BG, C.I. 42040, MW = 482.64 g/mol, λ_{max} = 625 nm) was purchased from BDH Chemicals [5]. Sodium chloride (NaCl), potassium chloride (KCl), and calcium carbonate ($CaCO_3$) were of analytical grade. All solutions were prepared using double-distilled water.

Preparation of nanoHydrogel XG-g-poly(PVP-co-AA-AAm)

Following the literature, free radical graft copolymerisation was used to synthesise the nanohydrogel [14,21]. By stirring at 60°C for 30 min, 0.1–1.0 g of xanthan gum was dissolved in 20 mL of distilled water. KPS initiator (0.01–0.1 g dissolved in 2 mL water) was added to produce free radicals. Next, PVP (0.1–1.0 g in 15 mL water), AAm (0.5–2.5 g in 2 mL water), and AA (1–10 mL) were added successively with continual stirring.

First, two drops of TEMED accelerator were added, then MBA (0.01–0.1 g in 2 mL water). For 15 min, nitrogen gas (N2) purged the mixture to eliminate dissolved oxygen. The reaction mixture was then placed in sealed glass tubes in a 70°C water bath for 2 h to polymerise [16]. After gelation, the nanohydrogel was cut into discs, washed eight times with distilled water at 30 min intervals to remove unreacted components, and dried in a 70°C oven. For adsorption investigations, dry discs were ground into fine, homogeneous particles.

Characterization

The crystalline structure of the nanohydrogel was analysed using a PANalytical X'Pert diffractometer with Cu Kα radiation (λ=1.5406 Å) at 40 kV and 30 mA [31]. The Shimadzu IR-Prestige spectrophotometer acquired FTIR spectra from 400 to 4000 cm^{-1} to confirm grafting and identify functional groups [32]. An SDT Q600 equipment was used to investigate thermal stability by TGA/DTA at 20°C/min in argon [33]. For surface morphology, a TESCAN MIRA3 LMU FESEM was used [34].

Batch Adsorption Experiments

Batch adsorption tests were done in 250 mL Erlenmeyer flasks with 50 mL BG dye solution at prescribed concentrations [10]. Add a known mass of nanohydrogel adsorbent and shake flasks in a temperature-controlled shaker. Contact time (0–220 min), pH (1.2–10), adsorbent dosage (0.0005–0.1 g), initial BG content (1–500 mg/L), ionic strength (0–0.2 mol/L NaCl, KCl, $CaCO_3$), and temperature (5–30°C) were assessed Periodically, aliquots were centrifuged and residual dye concentration determined at λmax = 625 nm using a UV-Vis spectrophotometer [5]. The calibration curve (Fig. 1) was established with excellent linearity (R^2 = 0.9983) for concentrations 0-50 mg/L. The adsorption capacity q_e (mg/g) and removal efficiency RE (%) were calculated using the following equations [10,11]:

$$q_e = \frac{V\,(C0 - Ce)}{m} \quad (1)$$

$$R_E\,(\%) = \frac{(C0 - Ce)}{C0} \times 100 \quad (2)$$

where C_0 and C_e are the initial and equilibrium dye concentrations (mg/L), V is the volume of solution (L), and m is the mass of adsorbent (g) [10].

RESULTS AND DISCUSSION

X-ray Diffraction (XRD) Analysis

The XRD pattern of the XG-g-poly(PVP-co-AA-AAm) nanohydrogel was obtained using a PANalytical X'Pert diffractometer at 40 kV, 30 mA, and Cu Kα radiation (λ = 1.5406 Å) (step size Fig. 2 shows a diffuse halo in the 2θ range of 15-30°,

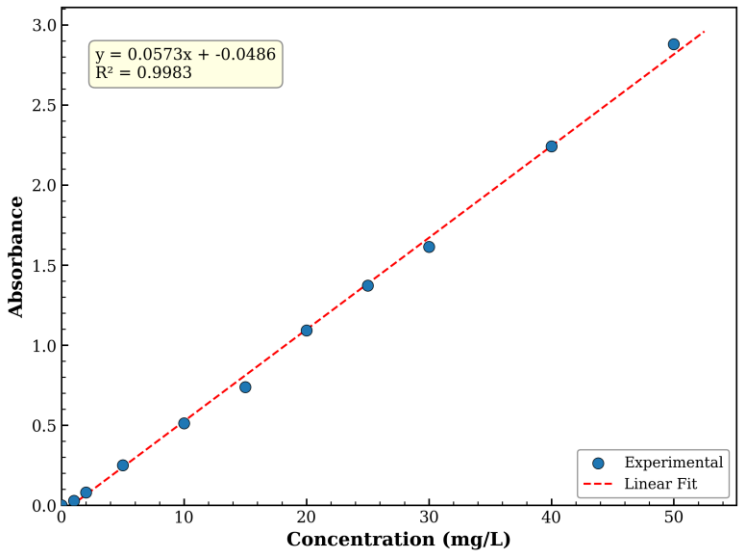

Fig. 1. Calibration curve of Brilliant Green dye at λmax = 625 nm (R^2 = 0.9983).

typical of amorphous polymeric materials [35] . MBA crosslinks disturb long-range crystalline periodicity, resulting in short-range order and random chain topologies in crosslinked hydrogel networks [36] . Semi-crystalline nature is shown by three diffraction peaks at 2θ = 19.18°, 20.68°, and 23.38° on the amorphous halo. The organised helical shape of the polysaccharide backbone and intermolecular hydrogen bonding create semi-crystalline domains of xanthan gum, which peak around 19.18° [37] . XRD evidence for native XG and its derivatives supports this position [38]. PVP's crystalline phase, showing a broad maximum near 2θ = 21° due to short-range molecular order in its pyrrolidone ring arrangement, is successfully incorporated into the copolymer, as indicated by the peak at 20.68°. Polyacrylamide segments display diffraction characteristics in the 22–24° region from hydrogen bonding between neighbouring amide groups, giving them the third peak at 23.38°. The amorphous halo dominates the crystalline peaks, indicating that grafting and crosslinking have drastically altered xanthan gum's inherent crystallinity. This primarily amorphous structure has better chain mobility, swelling capacity, and binding sites than highly crystalline polymers. The maintained semi-crystalline peaks provide structural integrity for adsorption-desorption [39].

Fourier-Transform Infrared Spectroscopy (FTIR) Analysis

FTIR identified functional groups and confirmed dye-adsorbent interactions. In Fig. 3, the virgin nanohydrogel (blue) and the nanohydrogel following BG adsorption (red) spectra are shown in the 400-4000 cm^{-1} range. The broad band at 3439 cm^{-1} in the pristine nanohydrogel spectra is caused by overlapping O–H and N–H stretching vibrations from xanthan gum hydroxyl, polyacrylamide amide, and PVP pyrrolidone ring [40]. The 2360 cm^{-1} band is due to asymmetric C-H stretching of methylene groups in the polymer backbone. The amide I C=O stretching exhibits a peak at 1647 cm^{-1}, with contributions from polyacrylamide, PVP carbonyl, and deprotonated acrylic acid's asymmetric carboxylate ($–COO^-$) stretching. The 1452 cm^{-1} band is caused by C–H scissoring of –CH2 groups and symmetric carboxylate stretching, whereas the 561 cm^{-1} absorption is due to polysaccharide backbone skeletal C–C vibrations [41]. After BG adsorption, various modifications occurred. The change in the O–H/N–H band from 3439 to 3434 cm^{-1} suggests hydrogen interaction between dye molecules and the nanohydrogel surface. Unionised –COOH groups caused a new band at 1712 cm^{-1}, indicating electrostatic charge neutralisation during dye uptake [42]. BG dye inclusion was confirmed by a 1514 cm^{-1} band,

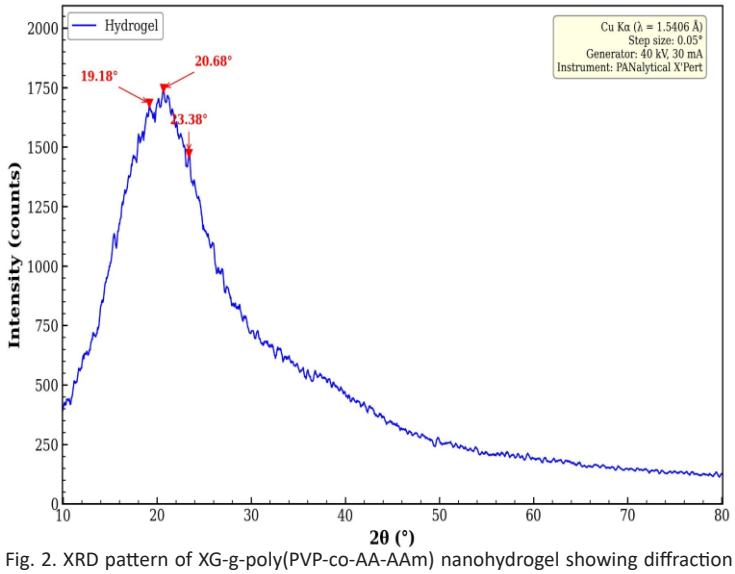

Fig. 2. XRD pattern of XG-g-poly(PVP-co-AA-AAm) nanohydrogel showing diffraction peaks at 2θ = 19.18°, 20.68°, and 23.38°.

indicating aromatic C=C ring stretching of the triphenylmethane structure. New bands at 1165 cm^{-1} (diethylamino group C–N stretching), 795 cm^{-1} (aromatic C–H out-of-plane bending), and 612 cm^{-1} (aromatic ring deformation) confirm BG adsorption [43]. Spectral shifts show that adsorption involves electrostatic interaction between the cationic dye and anionic carboxylate groups and hydrogen bonding with amide and hydroxyl functionalities [44].

Thermogravimetric and Differential Thermal Analysis (TGA/DTA)

Thermal stability was measured with an SDT Q600 under argon at 20°C/min over 30–700°C. In Fig. 4, the TGA/DTA data are shown in four panels. The TGA thermogram (Fig. 4a) shows three breakdown stages. Stage I (30–150°C) evaporation of physically adsorbed moisture in the nanohydrogel network causes 3.6% weight loss. Stage II (150–400°C) is the primary decomposition with 52.5% weight loss, involving glycosidic bond cleavage (250–350°C), NH3 elimination (>250°C), decarboxylation of poly(acrylic acid) chains (200–300°C), and PVP ring opening and chain scission (300–450°C) [45]. In Stage III (400–550°C), residual organic material carbonisation causes C–C bond rupture and volatile removal (CO, CO2, H2O) and 25.2% loss. Inorganic ash and carbonaceous char made up 14.8% of the residual at 700°C (85.2% loss [46]). In Fig. 4b, the DTA curve shows a glass transition temperature (Tg) of ~79°C, indicating the transition from glassy to rubbery state in amorphous polymer chains. The deepest endothermic peak is 279°C (–2.49 W/g), the primary decomposition event. Tangent analysis (Fig. 4c) showed onset = 234.3°C, peak = 279.2°C, and endset = 339.1°C, with a broad spread (ΔT = 104.8°C) indicating degradation of various polymeric components. TGA-DTA overlay (Fig. 4d) demonstrates wastewater treatment applications below 100°C are thermally stable. The multi-stage breakdown profile confirms several synthetic monomers grafting onto the polysaccharide backbone [47].

Field-Emission Scanning Electron Microscopy (FESEM) Analysis

Before and after BG dye adsorption, a TESCAN MIRA3 LMU FESEM with an InBeam detector evaluated surface morphology at different magnifications. The virgin nanohydrogel at 50.0 kx (Fig. 5a, 1 µm scale) has a rough, irregular surface with layered, folded characteristics and visible cracks, resembling crosslinked hydrogel networks [48]. Dye molecules diffuse into hydrogels through these pores. Particle size analysis showed $\bar{d}$ = 75.4 ± 50.9 nm (N = 451, median = 62.7 nm). At 200 kx (Fig. 5b, 200 nm scale), the surface is smooth and compact with rounded globular features ($\bar{d}$ = 91.9

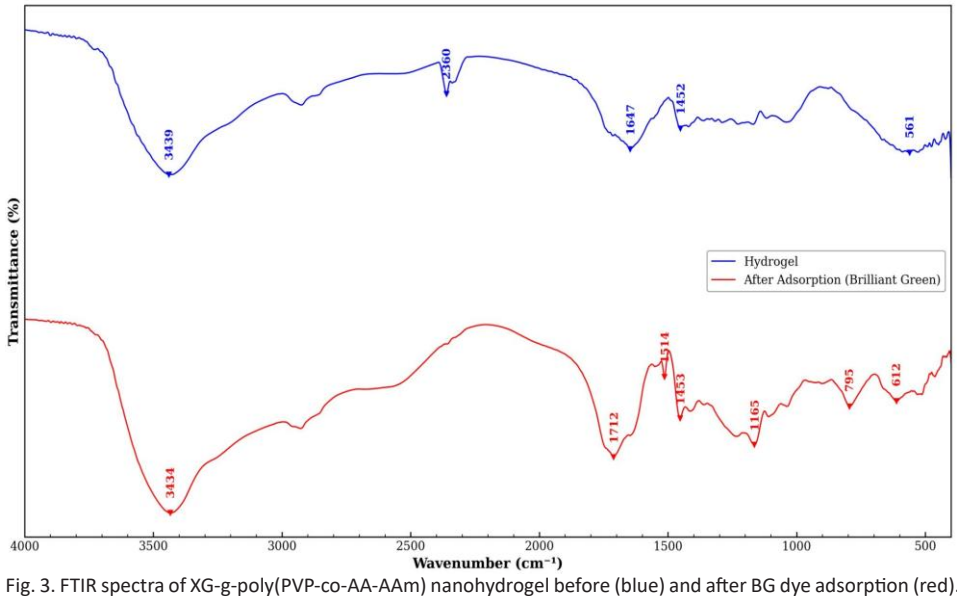

Fig. 3. FTIR spectra of XG-g-poly(PVP-co-AA-AAm) nanohydrogel before (blue) and after BG dye adsorption (red).

± 103.4 nm, N = 18), indicating nanoscale surface roughness and increased specific surface area. The shape changes drastically after BG adsorption. At 25.0 kx (Fig. 5c, 2 µm scale), the surface shows abundant spherical nanoparticles, unlike the pure nanohydrogel, indicating dye accumulation. The particle diameter grew significantly to 162.7 ± 135.6 nm (N = 488, median = 129.6 nm), indicating dye aggregation development. Individual spherical nanoparticles are clearly visible at 200 kx (Fig. 5d, 200 nm scale) with $\bar{d}$ = 29.7 ± 26.4 nm (N = 350, median = 17.1 nm These are electrostatic and hydrogen bonding-formed BG dye-polymer complex nodules. Wide size distributions match the Freundlich isotherm model's heterogeneous surface energy. Visually, the transition from smooth layered to nanoparticle-covered surfaces supports the high adsorption capacity (~37.3 mg/g) and >93% removal effectiveness [49].

Effect of Adsorbent Dosage

Fig. 6 shows how adsorbent dosage affected BG removal from 0.0005 to 0.1 g. As adsorbent mass grew, surface area and active sites increased, increasing adsorption capacity from 2.66 mg/g at 0.0005 g to 34.75 mg/g at 0.05 g. Qe decreased at dosages 0.08 and 0.1 g after the optimum 0.05 g. At high doses, adsorbent particles aggregate and overlap, reducing dye molecules' effective surface area and incompletely using binding sites [50]. The ratio of dye molecules to accessible sites falls at high adsorbent loadings, lowering per-unit-mass absorption. Mittal *et al.* and Sahiner et al. found similar optimum dose behaviour for dye adsorption onto waste materials and PDMAEMA hydrogels [51]. Trends show the necessity of optimising.

Effect of Contact Time

At 200 mg/L and 30°C, the effect of contact time on BG dye adsorption onto XG-g-poly(PVP-co-AA-AAm) nanohydrogel was examined from 0 to 220 min. Fig. 7 shows that the adsorption capacity grew fast within the first 15 min, reaching 37.15 mg/g and 92.86% removal efficiency. The nanohydrogel surface's many unoccupied active

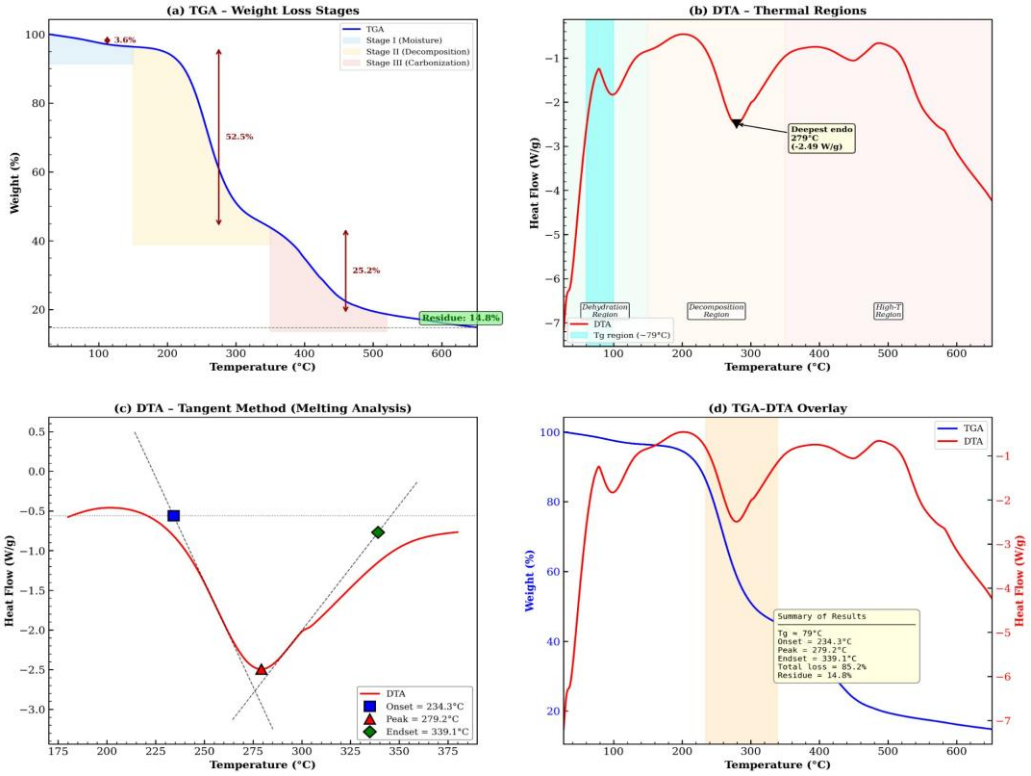

Fig. 4. TGA/DTA analysis: (a) TGA weight loss stages; (b) DTA thermal regions with Tg ≈ 79°C; (c) tangent method (onset 234.3°C, peak 279.2°C, endset 339.1°C); (d) TGA-DTA overlay.

sites and steep concentration gradient drive dye molecule mass transfer from the bulk solution to the adsorbent surface, resulting in rapid initial absorption [52]. Both methylene blue and malachite green have shown quick initial adsorption followed by gradual equilibration on carboxymethyl cellulose-based hydrogels and guar gum-grafted hydrogels [53]. After 60 min, adsorption slowed and reached equilibrium at 37.33 mg/g (93.34% removal) at 90 min. The minor rise up to 220 min was negligible, demonstrating that 90 min is a reasonable equilibrium time [54]. With equilibrium approaching, active site occupation and concentration gradient decrease explain progressive saturation. With fast adsorption kinetics, the XG-g-poly(PVP-co-AA-AAm) nanohydrogel is useful for wastewater treatment.

Effect of Solution pH

Adsorbent surface charge and dye molecule ionisation depend on solution pH. It was examined how pH affected BG adsorption from 1.2 to 10.0 (Fig. 8). From 37.05 mg/g at pH 1.2 to 38.03 mg/g at

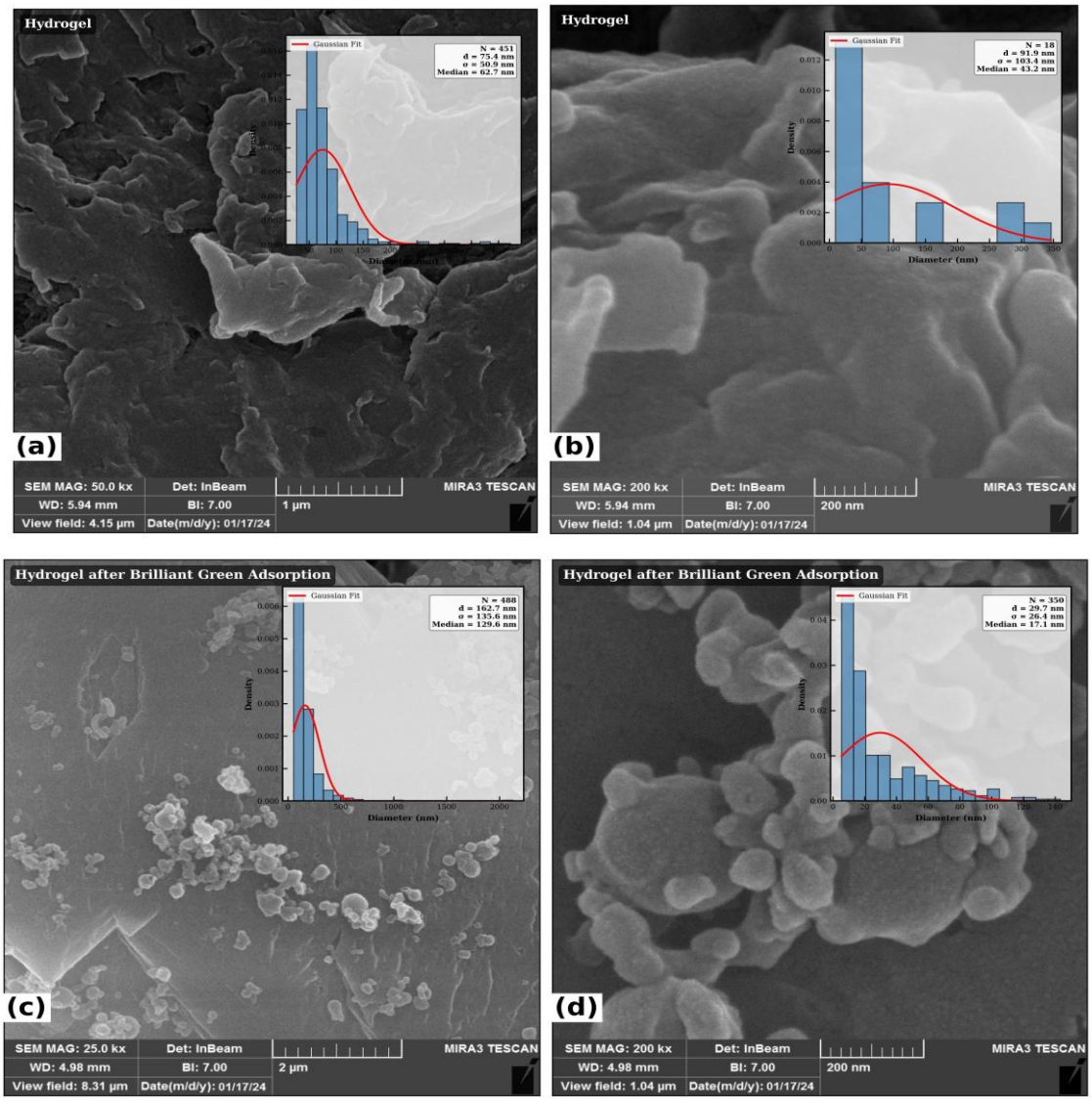

Fig. 5. FESEM of pristine nanohydrogel: (a) 50.0 kx (1 µm), $\bar{d}$ = 75.4 nm; (b) 200 kx (200 nm), $\bar{d}$ = 91.9 nm. FESEM after BG adsorption: (c) 25.0 kx (2 µm), $\bar{d}$ = 162.7 nm; (d) 200 kx (200 nm), $\bar{d}$ = 29.7 nm.

pH 10.0, adsorption capacity increased. At low pH, the nanohydrogel surface's carboxyl (–COOH) and amide (–CONH2) groups protonate, creating a net positive charge that repels cationic BG molecules and reduces adsorption. Increased pH above the pKa of acrylic acid (~4.25) [55] leads to carboxyl groups deprotonating to create carboxylate anions ($–COO^-$), enhancing electrostatic interaction between negatively charged nanohydrogel surface and positively charged BG cations. Reduced H+ ion competition for binding sites at high pH increases dye uptake. The monotonic increase in adsorption with pH emphasises the electrostatic character of the BG-hydrogel interaction and suggests pH 10 for maximal removal. This corresponds to cationic dye adsorption onto poly(acrylic acid)-based

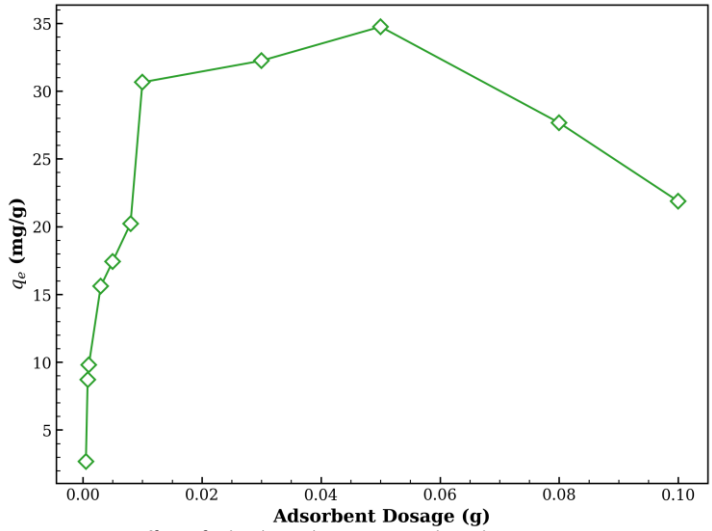

Fig. 6. Effect of adsorbent dosage on BG dye adsorption capacity.

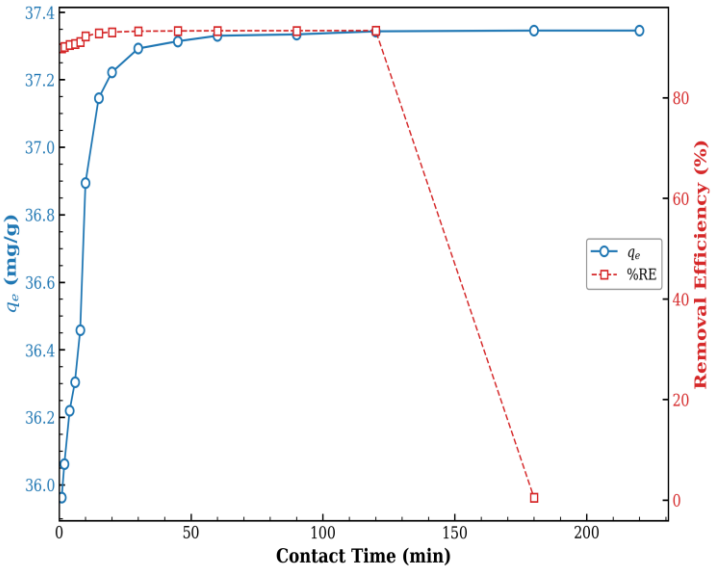

Fig. 7. Effect of contact time on BG dye adsorption capacity (qe) and removal efficiency (%RE) onto XG-g-poly(PVP-co-AA-AAm) nanohydrogel (C_o = 200 mg/L, T = 30°C).

adsorbents [56].

Adsorption Isotherms

Adsorption isotherms, which depict the balance between the adsorbate on the adsorbent and the remaining concentration in solution, are very important for understanding adsorption and making treatment systems. Isotherms were made at 15, 20, 30, and 40°C with BG concentrations from 1 to 500 mg/L (Fig. 9). The Giles classification [57] says that the isotherms were L-shaped, which means that they showed good adsorption and surface saturation at higher equilibrium concentrations. At all temperatures, the ability to adsorb increased with the original dye concentration. This is because mass transfer driving force is stronger at higher concentrations. Higher temperatures raised qe values at the same Ce, which supports the idea that adsorption is an endothermic process [58].

Fig. 10 shows three linearised classical isotherm models fitted to equilibrium data at 30°C. The

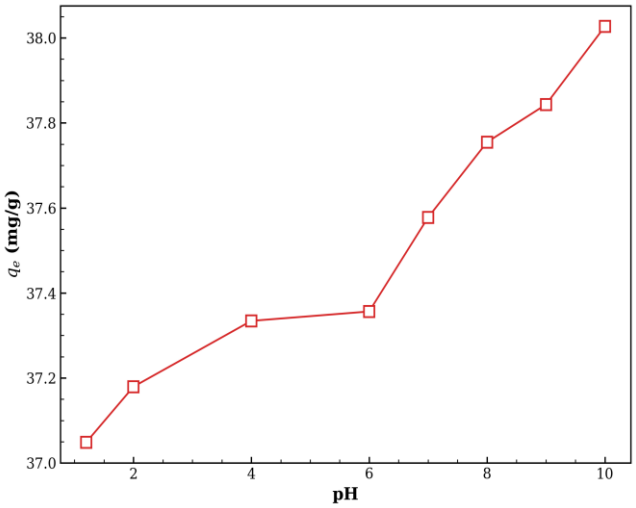

Fig. 8. Effect of solution pH on the adsorption capacity of BG dye onto XG-g-poly(PVP-co-AA-AAm) nanohydrogel.

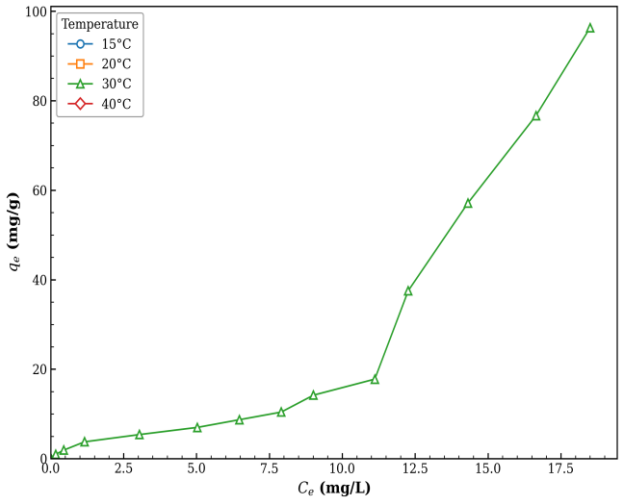

Fig. 9. Adsorption isotherms of BG dye on XG-g-poly(PVP-co-AA-AAm) nanohydrogel at different temperatures (15, 20, 30, and 40°C).

Langmuir model, which assumes monolayer coverage on a homogeneous surface, is expressed as:

$$C_e/q_e = 1/(K_L q_m) + C_e/q_m \quad (3)$$

The Freundlich model, which accounts for heterogeneous surface energies and multilayer adsorption, is given by:

$$\log q_e = \log K_F + (1/n) \log C_e \quad (4)$$

The Temkin model, which considers the effect of indirect adsorbent-adsorbate interactions on the adsorption process, is expressed as:

$$q_e = B \ln K_T + B \ln C_e \quad (5)$$

A low correlation coefficient ($R^2 = 0.2616$) in the Langmuir model ((Ce/qe) vs.(Ce)) suggests that adsorption does not behave as a monolayer on a homogenous surface Freundlich model (log(qe) vs. log(Ce)) provides a better fit (R^2=0.8209) with 1/n = 1.0026 and KF = 2.5483. 1/n around unity indicates a linear solution-adsorbent surface partition. Significant adsorption heat is shown by the intermediate correlation (R^2=0.4666) in the Temkin model (qe vs. lnCe) with B = 19.37 J/ XG-g-poly(PVP-co-AA-AAm) nanohydrogel surface is energetically heterogeneous because Freundlich model fits better, showing that numerous functional groups (carboxyl, amide, carbonyl, and hydroxyl) bind dye. Different polysaccharide-based hydrogels absorb cationic dyes Freundlich-like [59].

Adsorption Kinetics

The kinetic data were analyzed using pseudo-first-order (PFO) and pseudo-second-order (PSO) models to elucidate the rate-controlling mechanism of BG adsorption (Fig. 11 and Table 2). The PFO model, proposed by Lagergren [60], is expressed as:

$$\ln(q_e - q_t) = \ln q_e - k_1 t \quad (6)$$

The PSO model, developed by Ho and McKay [61], is given by:

$$t/q_t = 1/(k_2 q_e^{\,2}) + t/q_e \quad (7)$$

The PFO model displays low linearity (R^2 = 0.7015) and predicts qe of 1.89 mg/g, notably different from the experimental value of 37.35

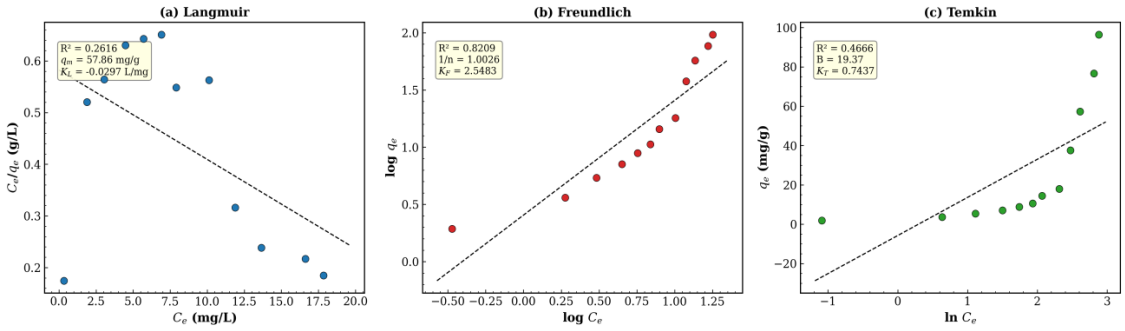

Fig. 10. Linear fits of (a) Langmuir, (b) Freundlich, and (c) Temkin isotherm models for BG adsorption at 30°C.

Table 1. Isotherm model parameters for BG dye adsorption onto XG-g-poly(PVP-co-AA-AAm) nanohydrogel at 30°C.

Model	Parameter	Value	R^2
Langmuir	qm (mg/g)	57.86	0.2616
	KL (L/mg)	–0.0297	
Freundlich	1/n	1.0026	0.8209
	KF	2.5483	
Temkin	B (J/mol)	19.37	0.4666
	KT	0.7437	

mg/g. This contradiction proves the PFO model cannot explain this system's adsorption behaviour. In comparison, the PSO model exhibited a linear fit with R^2=1.000. Experimental and calculated equilibrium adsorption capacities (qe,calc = 37.31 mg/g) matched. The rate constant k_2=0.2687 g/mg·min and initial adsorption rate h = $k_2 qe^2$ = 375.19 mg/g·min indicate rapid absorption in trials. The more applicable PSO model demonstrates that chemisorption, involving valence forces through electron sharing or exchange between dye molecules and nanohydrogel functional groups, is the rate-limiting phase [62]. This matches polysaccharide-based hydrogel cationic dye adsorption.

Intraparticle Diffusion Model (Weber-Morris)

The intraparticle diffusion model proposed by Weber and Morris was applied [63] to further investigate the diffusion mechanism governing the adsorption of Brilliant Green dye onto the XG-g-poly(PVP-co-AA-AAm) nanohydrogel. This model is expressed as:

$$q_t = k_{id}\, t^{0.5} + C \quad (8)$$

where q_t (mg/g) is the amount of dye adsorbed at time t (min), k_{id} (mg/g·min$^{0.5}$) is the intraparticle diffusion rate constant obtained from the slope of the linear plot of q_t versus $t^{0.5}$, and C (mg/g) is the intercept, which provides an indication of the thickness of the boundary layer. If intraparticle diffusion is the sole rate-controlling step, the plot of q_t versus $t^{0.5}$ should yield a straight line passing through the origin (C = 0). Deviation of the intercept from zero indicates that the adsorption process is governed by multiple mechanisms, with boundary layer diffusion also playing a significant role.

The linear regression of qt against t0.5 revealed an intraparticle diffusion rate constant (kid) of 0.0936 mg/g·min0.5, an intercept (C) of 36.3445

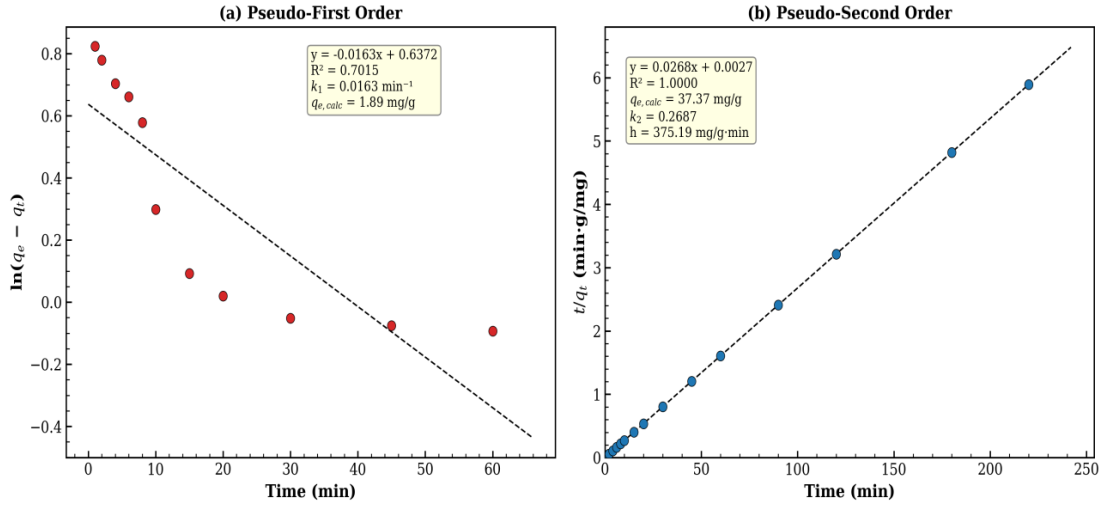

Fig. 11. Kinetic model plots: (a) pseudo-first-order and (b) pseudo-second-order for BG adsorption on XG-g-poly(PVP-co-AA-AAm) nanohydrogel.

Table 2. Kinetic parameters for BG dye adsorption onto XG-g-poly(PVP-co-AA-AAm) nanohydrogel.

Model	Parameter	Value	R^2
PFO	k_1 (min^{-1})	0.0163	0.7015
	qe,calc (mg/g)	1.89	
PSO	k_2 (g/mg·min)	0.2687	1.0000
	qe,calc (mg/g)	37.31	
	h (mg/g·min)	375.19	
Experimental	qe,exp (mg/g)	37.35	—

mg/g, and a correlation coefficient (R^2) of 0.5906 (Table 3, Fig. 12). The low R^2 value shows that the way BG dye gets into the nanohydrogel is not through a single-step intraparticle diffusion mechanism, but rather through many mass transfer stages. The most relevant result of this study is the intercept C (36.3445 mg/g). Weber and Morris say that the figure should go through the origin if intraparticle diffusion is the only step that slows down the process. The strong positive intercept indicates that boundary layer diffusion (external film diffusion) has an impact on the rate of adsorption, particularly in the first stages. The boundary layer effect has a direct impact on C; the broader the intercept, the more surface adsorption occurs in the step that controls the rate. C = 36.3445 mg/g is 97.3% of the equilibrium adsorption capacity (qe,exp = 37.35 mg/g). This means that most of the dye is taken up by the exterior boundary layer quickly before it diffuses into the particles. The pseudo-second-order kinetic data, which are quite similar (R^2 = 1.000), confirm chemisorption as the main mechanism. The contact time experiments demonstrated swift initial absorption (92.86% elimination within 15 minutes), corroborating surface-mediated interactions such as electrostatic attraction between the cationic BG dye and the anionic carboxylate groups, as well as hydrogen bonding with the nanohydrogel's amide and hydroxyl functionalities. Intraparticle diffusion aids the system in achieving equilibrium; however, it is not the primary rate-limiting process. Because there are functional groups on the surface, boundary layer effects are the main reason cationic dyes stick to polysaccharide-based hydrogels.

Thermodynamic Studies

The energetics and spontaneity of adsorption are revealed by thermodynamic parameters.

Table 3. Intraparticle diffusion model parameters.

Parameter	Value	Unit
kid	0.0936	mg/g·min^{1φ2}
C (intercept)	36.3445	mg/g
R^2	0.5906	—
qe,exp	37.35	mg/g

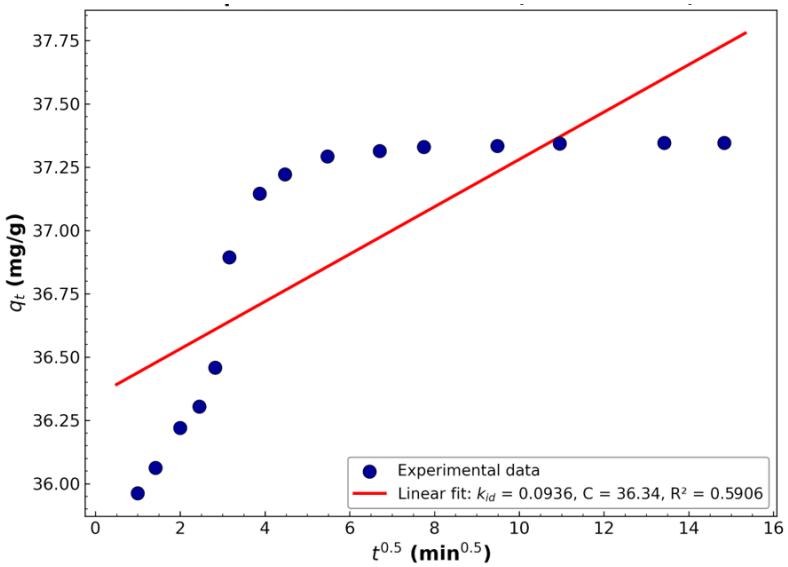

Fig. 12. Intraparticle diffusion plot (qt vs. $t^{1φ2}$) for BG dye adsorption onto XG-g-poly(PVP-co-AA-AAm) nanohydrogel.

Adsorption isotherms were obtained at 5, 10, 20, and 30°C (Fig. 13), and thermodynamic values were calculated using the Van't Hoff plot of ln Kd versus 1000/T (Fig. 14). The distribution coefficient Kd was qe/Ce at each temperature. The standard Gibbs free energy change (ΔG°), enthalpy change (ΔH°), and entropy change (ΔS°) were evaluated using the following thermodynamic equations:

$$\Delta G^\circ = -RT \ln K_d \quad (9)$$

$$\ln K_d = \Delta S^\circ/R - \Delta H^\circ/RT \quad (10)$$

The linear Van't Hoff plot showed ΔH° = 4.99 kJ/mol and ΔS° = 54.20 J/mol·K as the slope and intercept. Increased absorption at higher temperatures supports the endothermic

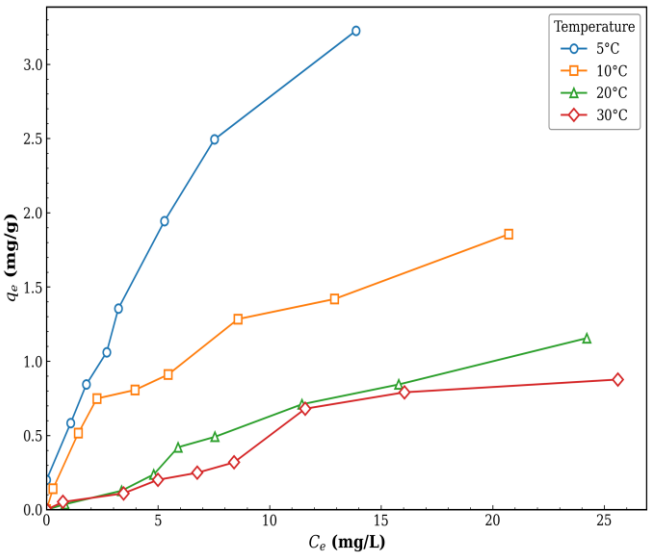

Fig. 13. Adsorption isotherms of BG dye at different temperatures (5, 10, 20, and 30°C).

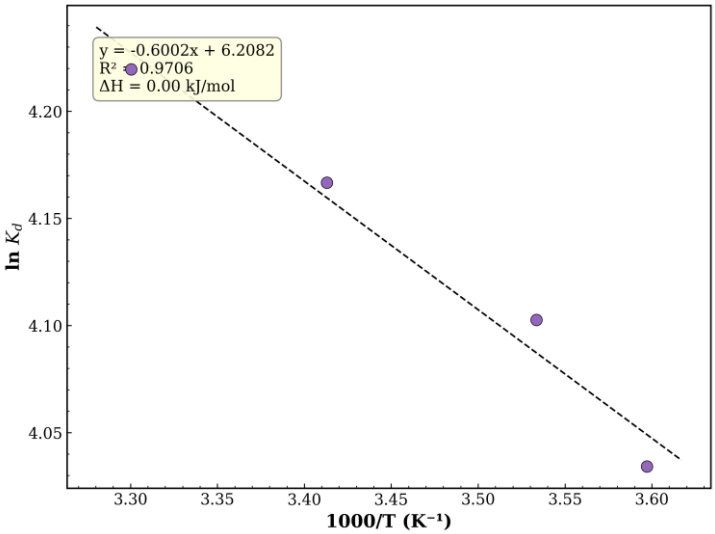

Fig. 14. Van't Hoff plot (ln Kd vs. 1000/T) for BG dye adsorption onto XG-g-poly(PVP-co-AA-AAm) nanohydrogel.

Table 4. Thermodynamic parameters for BG dye adsorption onto XG-g-poly(PVP-co-AA-AAm) nanohydrogel.

T (°C)	T (K)	ΔG° (kJ/mol)	ΔH° (kJ/mol)	ΔS° (J/mol·K)
5	278	–10.89	4.99	54.20
10	283	–11.16		
20	293	–11.70		
30	303	–12.24		

character of the adsorption process, as indicated by the positive ΔH° value. The high ΔH° (< 40 kJ/mol) indicates a physical adsorption mechanism with added weak chemical forces. The positive ΔS° reflects increased randomness at the solid-solution interface during adsorption, possibly due to the release of structured water molecules from the nanohydrogel matrix as dye molecules penetrate the swollen network. The process is spontaneous and thermodynamically favourable (Table 4), as evidenced by the negative ΔG° values at all temperatures (ΔG° = –10.89 kJ/mol at 278 K) Lower ΔG° results (–10.89 to –12.24 kJ/mol from 5 to 30°C) suggest increased spontaneity at higher temperatures, supporting endothermic behaviour. The thermodynamic behaviour of Rhodamine B on Raphia hookeri fruit epicarp and crystal violet on alginate-based hydrogels is similar [64].

CONCLUSION

A new XG-g-poly(PVP-co-AA-AAm) nanohydrogel was synthesised and tested for Brilliant Green dye removal from water. XRD showed a mostly amorphous structure with semi-crystalline peaks at 19.18°, 20.68°, and 23.38°. FTIR confirmed effective grafting and dye adsorption via new bands at 1514, 1712, and 1165 cm^{-1}. Thermal stability was good for TGA/DTA, with breakdown at 234.3°C and Tg = 79°C. FESEM showed dye deposition through spherical nanoparticles on the nanohydrogel surface following adsorption. With optimum circumstances (C_o = 200 mg/L, dosage = 0.005 g, natural pH, 30°C), the nanohydrogel achieved 37.33 mg/g adsorption capacity and 93.34% removal efficiency in 90 minutes. Kinetics confirmed chemisorption as the primary process, following the pseudo-second-order model (R^2 = 1.000). The Weber-Morris model showed boundary layer and intraparticle diffusion. Freundlich isotherm best fit equilibrium data, indicating heterogeneous multilayer adsorption. Sudden, endothermic adsorption with increased solid-liquid interface unpredictability was confirmed by thermodynamic parameters. The nanohydrogel performed well with competing electrolytes. This shows that the XG-g-poly(PVP-co-AA-AAm) nanohydrogel is a potential, eco-friendly cationic dye-contaminated wastewater adsorbent.

CONFLICT OF INTEREST

The authors declare that there is no conflict of interests regarding the publication of this manuscript.

REFERENCES

1. Ahmad MA, Ahmad N, Bello OS. Adsorptive Removal of Malachite Green Dye Using Durian Seed-Based Activated Carbon. Water, Air and Soil Pollution. 2014;225(8).
2. Gupta VK, Suhas. Application of low-cost adsorbents for dye removal – A review. J Environ Manage. 2009;90(8):2313-2342.
3. Yagub MT, Sen TK, Afroze S, Ang HM. Dye and its removal from aqueous solution by adsorption: A review. Advances in Colloid and Interface Science. 2014;209:172-184.
4. Kant R. Textile dyeing industry an environmental hazard. Natural Science. 2012;04(01):22-26.
5. Ghaedi M, Ansari A, Habibi MH, Asghari AR. Removal of malachite green from aqueous solution by zinc oxide nanoparticle loaded on activated carbon: Kinetics and isotherm study. Journal of Industrial and Engineering Chemistry. 2014;20(1):17-28.
6. Mittal A, Mittal J, Malviya A, Gupta VK. Removal and recovery of Chrysoidine Y from aqueous solutions by waste materials. Journal of Colloid and Interface Science. 2010;344(2):497-507.
7. Forgacs E, Cserháti T, Oros G. Removal of synthetic dyes from wastewaters: a review. Environ Int. 2004;30(7):953-971.
8. Verma AK, Dash RR, Bhunia P. A review on chemical coagulation/flocculation technologies for removal of colour from textile wastewaters. J Environ Manage. 2012;93(1):154-168.
9. Holkar CR, Jadhav AJ, Pinjari DV, Mahamuni NM, Pandit AB. A critical review on textile wastewater treatments: Possible approaches. J Environ Manage. 2016;182:351-366.
10. Inyinbor AA, Adekola FA, Olatunji GA. Kinetics, isotherms and thermodynamic modeling of liquid phase adsorption of Rhodamine B dye onto Raphia hookerie fruit epicarp. Water Resources and Industry. 2016;15:14-27.
11. Wong YC, Szeto YS, Cheung WH, McKay G. Adsorption of acid dyes on chitosan—equilibrium isotherm analyses. Process Biochem. 2004;39(6):695-704.
12. Rafatullah M, Sulaiman O, Hashim R, Ahmad A. Adsorption

of methylene blue on low-cost adsorbents: A review. J Hazard Mater. 2010;177(1-3):70-80.
13. Crini G. Non-conventional low-cost adsorbents for dye removal: A review. Bioresour Technol. 2006;97(9):1061-1085.
14. Dragan ES. Design and applications of interpenetrating polymer network hydrogels. A review. Chem Eng J. 2014;243:572-590.
15. Sahiner N, Demirci S, Sahiner M, Yilmaz S. Application of superporous magnetic cationic cryogels for persistent chromate (toxic chromate and dichromate) uptake from aqueous environments. J Appl Polym Sci. 2016;133(20).
16. Sharma S, Dua A, Malik A. Polyaspartic acid based superabsorbent polymers. Eur Polym J. 2014;59:363-376.
17. Shang J, Shao Z, Chen X. Electrical Behavior of a Natural Polyelectrolyte Hydrogel: Chitosan/Carboxymethylcellulose Hydrogel. Biomacromolecules. 2008;9(4):1208-1213.
18. Wang W, Wang A. Synthesis and swelling properties of pH-sensitive semi-IPN superabsorbent hydrogels based on sodium alginate-g-poly(sodium acrylate) and polyvinylpyrrolidone. Carbohydr Polym. 2010;80(4):1028-1036.
19. García-Ochoa F, Santos VE, Casas JA, Gómez E. Xanthan gum: production, recovery, and properties. Biotechnol Adv. 2000;18(7):549-579.
20. Kumar A, Rao KM, Han SS. Application of xanthan gum as polysaccharide in tissue engineering: A review. Carbohydr Polym. 2018;180:128-144.
21. Mahdavinia GR, Massoudi A, Baghban A, Shokri E. Study of adsorption of cationic dye on magnetic kappa-carrageenan/PVA nanocomposite hydrogels. Journal of Environmental Chemical Engineering. 2014;2(3):1578-1587.
22. Zendehdel M, Barati A, Alikhani H. Preparation and characterization of poly(acryl amide-coacrylic acid)/nay and Clinoptilolite nanocomposites with improved methylene blue dye removal behavior from aqueous solution. nano Online: De Gruyter; 2016.
23. Kyzas G, Bikiaris D. Recent Modifications of Chitosan for Adsorption Applications: A Critical and Systematic Review. Mar Drugs. 2015;13(1):312-337.
24. Dhodapkar R, Rao NN, Pande SP, Nandy T, Devotta S. Adsorption of cationic dyes on Jalshakti®, super absorbent polymer and photocatalytic regeneration of the adsorbent. React Funct Polym. 2007;67(6):540-548.
25. Garg VK, Kumar R, Gupta R. Removal of malachite green dye from aqueous solution by adsorption using agro-industry waste: a case study of Prosopis cineraria. Dyes and Pigments. 2004;62(1):1-10.
26. Lipietz A. The so-called "transformation problem" revisited. Journal of Economic Theory. 1982;26(1):59-88.
27. Ho YS, McKay G. Pseudo-second order model for sorption processes. Process Biochem. 1999;34(5):451-465.
28. Langmuir I. The Constitution and Fundamental Properties of Solids and Liquids. Part I. Solids. Journal of the American Chemical Society. 1916;38(11):2221-2295.
29. Freundlich H. Über die Adsorption in Lösungen. Z Phys Chem. 1907;57U(1):385-470.
30. Sasa Y, Uda M, Toyoshima I. The Crystallite Size Of A-Iron in the Presence of K2O In The Doubly Promoted Ammonia Synthesis Iron Catalysts. Chem Lett. 1982;11(12):2011-2014.
31. Julnes G. Evaluation (2nd Edition), by Carol Hirshon Weiss, Upper Saddle River, NJ: Prentice Hall, 1998, 372 pp. The American Journal of Evaluation. 2001;22(2):265-268.
32. Jennings KR. Spectrometric identification of organic compounds (Fifth Edition) R. M. SILVERSTEIN, G. C. BASSLER AND T. C. MORRILL. Wiley, New York, 1991. No. of pages: 430. ISBN 0471 63404 2. Price: £50.25, $76.10. Org Mass Spectrom. 1991;26(9):813-813.
33. Principles and Applications of Thermal Analysis: Wiley; 2008.
34. Goldstein JI, Newbury DE, Echlin P, Joy DC, Lyman CE, Lifshin E, et al. Scanning Electron Microscopy and X-ray Microanalysis. Springer US; 2003.
35. Thakur S, Govender PP, Mamo MA, Tamulevicius S, Mishra YK, Thakur VK. Progress in lignin hydrogels and nanocomposites for water purification: Future perspectives. Vacuum. 2017;146:342-355.
36. Peppas N. Hydrogels in pharmaceutical formulations. Eur J Pharm Biopharm. 2000;50(1):27-46.
37. Torres FG, Troncoso OP, Pisani A, Gatto F, Bardi G. Natural Polysaccharide Nanomaterials: An Overview of Their Immunological Properties. Int J Mol Sci. 2019;20(20):5092.
38. Kumar A, Singh K, Ahuja M. Xanthan-g-poly(acrylamide): Microwave-assisted synthesis, characterization and in vitro release behavior. Carbohydr Polym. 2009;76(2):261-267.
39. Mahdavinia GR, Iravani S, Zoroufi S, Hosseinzadeh H. Magnetic and K+-cross-linked kappa-carrageenan nanocomposite beads and adsorption of crystal violet. Iranian Polymer Journal. 2014;23(5):335-344.
40. Abou Taleb MF, Mahmoud GA, Elsigeny SM, Hegazy E-SA. Adsorption and desorption of phosphate and nitrate ions using quaternary (polypropylene-g-N,N-dimethylamino ethylmethacrylate) graft copolymer. J Hazard Mater. 2008;159(2-3):372-379.
41. Wang L, Zhang J, Wang A. Fast removal of methylene blue from aqueous solution by adsorption onto chitosan-g-poly (acrylic acid)/attapulgite composite. Desalination. 2011;266(1-3):33-39.
42. Vimonses V, Lei S, Jin B, Chow CWK, Saint C. Kinetic study and equilibrium isotherm analysis of Congo Red adsorption by clay materials. Chem Eng J. 2009;148(2-3):354-364.
43. Ghaemy M, Amini Nasab SM. Synthesis and identification of organosoluble polyimides: thermal, photophysical and chemiluminescence properties. Polym J. 2010;42(8):648-656.
44. Namdeo M, Bajpai SK. Immobilization of α-amylase onto cellulose-coated magnetite (CCM) nanoparticles and preliminary starch degradation study. J Mol Catal B: Enzym. 2009;59(1-3):134-139.
45. Chauhan GS, Mahajan S, Guleria LK. Polymers from renewable resources: sorption of Cu^{2+} ions by cellulose graft copolymers. Desalination. 2000;130(1):85-88.
46. Soares JdP, Dos Santos JE, Chierice GO, Cavalheiro ÉTG. Thermal behavior of alginic acid and its sodium salt. Ecletica Quimica. 2004;29(2):57-63.
47. Sharma K, Kaith BS, Kumar V, Kalia S, Kumar V, Swart HC. Synthesis and biodegradation studies of gamma irradiated electrically conductive hydrogels. Polymer Degradation and Stability. 2014;107:166-177.
48. Dragan ES, Dinu MV, Timpu D. Preparation and characterization of novel composites based on chitosan and clinoptilolite with enhanced adsorption properties for Cu^{2+}. Bioresour Technol. 2010;101(2):812-817.
49. Liu Y, Zheng Y, Wang A. Enhanced adsorption of Methylene Blue from aqueous solution by chitosan-g-poly (acrylic

acid)/vermiculite hydrogel composites. Journal of Environmental Sciences. 2010;22(4):486-493.
50. Mittal H, Ray SS, Kaith BS, Bhatia JK, Sukriti, Sharma J, et al. Recent progress in the structural modification of chitosan for applications in diversified biomedical fields. Eur Polym J. 2018;109:402-434.
51. Sahiner N, Demirci S, Sahiner M, Yilmaz S, Al-Lohedan H. The use of superporous p(3-acrylamidopropyl)trimethyl ammonium chloride cryogels for removal of toxic arsenate anions. J Environ Manage. 2015;152:66-74.
52. Reddad Z, Gerente C, Andres Y, Le Cloirec P. Adsorption of Several Metal Ions onto a Low-Cost Biosorbent: Kinetic and Equilibrium Studies. Environmental Science and Technology. 2002;36(9):2067-2073.
53. Singh V, Tripathi DN, Tiwari A, Sanghi R. Microwave synthesized chitosan-graft-poly(methylmethacrylate): An efficient Zn2+ ion binder. Carbohydr Polym. 2006;65(1):35-41.
54. Pourjavadi A, Sadeghi M, Hosseinzadeh H. Modified carrageenan. 5. Preparation, swelling behavior, salt- and pH-sensitivity of partially hydrolyzed crosslinked carrageenan-graft-polymethacrylamide superabsorbent hydrogel. Polym Adv Technol. 2004;15(11):645-653.
55. Rivas B. Water-soluble polymer–metal ion interactions. Prog Polym Sci. 2003;28(2):173-208.
56. Wan Ngah WS, Teong LC, Hanafiah MAKM. Adsorption of dyes and heavy metal ions by chitosan composites: A review. Carbohydr Polym. 2011;83(4):1446-1456.
57. Giles CH, MacEwan TH, Nakhwa SN, Smith D. 786. Studies in adsorption. Part XI. A system of classification of solution adsorption isotherms, and its use in diagnosis of adsorption mechanisms and in measurement of specific surface areas of solids. Journal of the Chemical Society (Resumed). 1960:3973.
58. Lima ÉC, Adebayo MA, Machado FM. Kinetic and Equilibrium Models of Adsorption. Carbon Nanostructures: Springer International Publishing; 2015. p. 33-69.
59. Mahdavinia GR, Asgari A. Synthesis of kappa-carrageenan-g-poly(acrylamide)/sepiolite nanocomposite hydrogels and adsorption of cationic dye. Polym Bull. 2013;70(8):2451-2470.
60. Bruzelius RM. Bidrag till kannedomen om Skandinaviens Amphipoda Gammaridea. Kungl Svenska vetenskapsakademiens handlingar. 1859;3:1-104.
61. Ho YS, McKay G. Sorption of dyes and copper ions onto biosorbents. Process Biochem. 2003;38(7):1047-1061.
62. Ho Y. The kinetics of sorption of divalent metal ions onto sphagnum moss peat. Water Res. 2000;34(3):735-742.
63. Weber WJ, Morris JC. Kinetics of Adsorption on Carbon from Solution. Journal of the Sanitary Engineering Division. 1963;89(2):31-59.
64. Bello OS, Adegoke KA, Akinyunni OO. Preparation and characterization of a novel adsorbent from Moringa oleifera leaf. Applied Water Science. 2015;7(3):1295-1305.